Abdominal Radiology

Published online: 22 August 2018

Abdom Radiol (2019) 44:756–765
https://doi.org/10.1007/s00261-018-1748-0

Combined application of virtual monoenergetic high keV images and the orthopedic metal artifact reduction algorithm (O-MAR): effect on image quality

Junghoan Park,[1,2] Se Hyung Kim,[1,2] and Joon Koo Han[1,2,3]

[1]Department of Radiology, Seoul National University Hospital, 101 Daehak-ro, Jongno-gu, Seoul 03080, Republic of Korea
[2]Seoul National University College of Medicine, Seoul, Republic of Korea
[3]Institute of Radiation Medicine, Seoul National University Medical Research Center, Seoul, Republic of Korea

Abstract

Purpose: To determine whether there is any additional metal artifact reduction when virtual monochromatic images (VMI) and metal artifact reduction for orthopedic implants (O-MAR) are applied together compared to their separate application in both phantom and clinical abdominopelvic CT studies.
Methods: An agar phantom containing a spinal prosthesis was scanned using a dual-layer, energy CT scanner (IQon, Philips Healthcare), and reconstructed with the filtered back-projection algorithm without O-MAR (FBP), filtered back-projection algorithm with O-MAR (O-MAR), VMI_{140} without O-MAR (VMI_{140}), and VMI_{140} with O-MAR (VMI_{140} + O-MAR). Abdominopelvic CT images of 47 patients with metallic prostheses were also reconstructed in the same manner for clinical study. Noise measured as the standard deviation of CT Hounsfield units was compared between the four reconstruction methods in both phantom and clinical studies. Improvements in metal artifact reduction, image quality, and diagnostic improvement were further analyzed in the clinical study.
Results: Noise was significantly decreased when both VMI and O-MAR were applied in conjunction compared to their separate application in both phantom (16.3 HU vs. 25.0 and 26.4 HU) and clinical studies (15.8 HU vs. 19.2 and 26.2 HU). In the clinical study, the qualitative degree of artifacts was also significantly reduced with VMI_{140} + O-MAR (2.85 and 2.87) compared to VMI_{140} (2.36 and 2.26) or O-MAR (2.13 and 2.04) alone for both reviewers ($P < 0.001$) and improvements in image quality were observed in all 47 patients, with actual diagnostic improvements observed in three.
Conclusions: Metal artifacts can be additionally reduced by applying O-MAR and VMI in conjunction, compared to their separate application, thereby improving diagnostic performance.

Key words: Metal artifact—Dual-energy CT—Virtual monoenergetic image—Artifact reduction

Metal artifacts are one of the major sources that worsen the diagnostic quality of CT images not only in the diagnosis and follow-up of musculoskeletal disorders but also in abdominal and pelvic diseases. Metal artifacts are caused by two major sources, beam-hardening and photon starvation effects [1–4]. The beam-hardening effect is caused by the polychromatic nature of X-ray beams used in CT, which means that the mean energy of the beam is increased as lower energy photons are more easily absorbed than higher energy photons. This leads to non-linear X-ray absorption, which in turn can lead to cupping and streak artifacts [2, 3]. Photon starvation, on the other hand, occurs when an X-ray beam passes through a highly attenuated area, where only insufficient photons reach the detector, producing very noisy projections. It is also a major source of streak artifacts [2, 4].

Various attempts have been made to reduce such metal artifacts including the application of iterative reconstruction algorithms [5–9] and the use of virtual monochromatic images (VMI) on dual-energy CT [1, 10–14]. Iterative reconstruction methods utilize an iterative loop that repeats the process of estimating the projection error related to high-density objects and correcting this

Correspondence to: Se Hyung Kim; *email:* shkim7071@gmail.com

image by subtracting the projection error [8, 9]. Metal artifact reduction for orthopedic implants (O-MAR, Philips Medical Systems, The Netherlands), one of the commercially available algorithms using the iterative reconstruction method, has shown to reduce metal artifacts and has shown an improved diagnostic performance in its application of abdominal CT [7, 15–17].

VMI is another powerful method that can help reduce metal artifacts. It is well known that CT images of different monochromatic X-ray beam energies or VMIs can be synthesized from dual-energy CT scans using either projection- or image-based methods [11, 13], and that these resultant synthesized monochromatic images would have no beam-hardening artifacts theoretically. Indeed, several reports have already revealed that virtual monochromatic images with an optimal energy between 95 and 150 keV would have the potential to reduce these metal artifacts [1, 11, 12].

There have been a few reports comparing VMI and iterative reconstruction method on reducing metal artifacts [18–20]. According to the previous reports, both VMI and iterative reconstruction method performed well in metal artifact reduction, but VMI seems to be less effective than iterative reconstruction method for large orthopedic implants [18–20]. However, VMI has the advantage of reducing metal artifacts without generating new artifacts while the iterative reconstruction method including O-MAR produces secondary artifacts [18]. Therefore, if VMI is combined with O-MAR, metal artifact may be further reduced without increasing secondary artifact compared to O-MAR alone.

At present, however, although VMI and O-MAR can be applied together using a single commercialized CT scanner, it is not yet known whether any additional metal artifact reduction can be obtained when using VMI and O-MAR together. Therefore, the purpose of this study was to evaluate whether there is any additional metal artifact reduction when VMI and O-MAR are applied together as compared to when they are separately applied in both a phantom and clinical abdominopelvic CT study.

Materials and methods

The institutional review board of our hospital approved this clinical abdominopelvic study and the requirement for informed consent was waived due to the retrospective nature of this study. None of the investigators in this study was an employee of or a consultant to the company that produced the VMI and O-MAR algorithm, and the authors had complete control of all data and information included in this study.

Phantom study

Phantom design

An agar phantom simulating the retroperitoneal space containing a spinal prosthesis was designed according to a previous study by Jeong et al. [17]. The agar phantom contained two sets of spinal screws placed obliquely at 45° angles, and two sticks of sausages and two sticks of rice cakes which simulated the retroperitoneal lymph nodes and large vessels, respectively (Fig. 1). The phantom was then submerged into a 1:100 solution of diatrizoate meglumine (660 mg/mL) and diatrizoate sodium (100 mg/mL) (Gastrografin, Bracco Diagnostics, Italy) approximating an attenuation of 100 Hounsfield units (HU).

CT acquisition

CT examinations were performed using a dual-layer, dual-energy CT scanner (IQon spectral CT, Philips Healthcare, Best, The Netherlands). The scanning parameters were as follows: detector configurations, 64 × 0.625 mm; tube voltage, 120 kVp; tube current, 51 mAs; pitch, 0.797; rotation time: 0.33 s; matrix, 512 × 512; slice thickness, 3 mm; and reconstruction interval, 2 mm. To evaluate the effect of VMI and O-MAR in metal artifact reduction, images were reconstructed using the following four methods: (1) filtered back-projection algorithm without O-MAR (FBP), (2) filtered back-projection algorithm with O-MAR (O-MAR), (3) VMI_{140} without O-MAR (VMI_{140}), and (4) VMI_{140} with O-MAR (VMI_{140} + O-MAR). An optimal

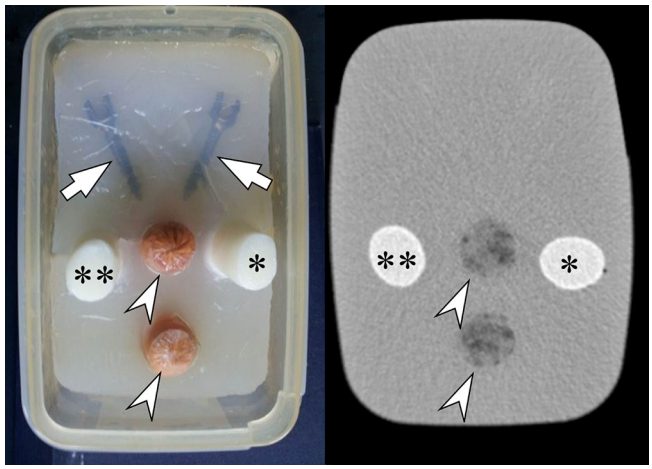

Fig. 1. Photograph (left) and CT image (right) of an agar phantom simulating the retroperitoneal space containing a spinal prosthesis. The phantom contains two sets of spinal screws (arrows) placed obliquely at 45° angles, two sticks of sausages (arrowheads) simulating retroperitoneal lymph nodes, and two sticks of rice cakes stimulating large vessels such as the aorta (**) and inferior vena cava (*). The phantom was submerged into a 1:100 solution of diatrizoate meglumine (660 mg/mL) and diatrizoate sodium (100 mg/mL) (Gastrografin, Bracco Diagnostics, Italy) with an attenuation of approximately 100 Hounsfield units (HU).

energy of 140 keV was selected to generate VMI as described in a previous study [21].

CT image analysis

Noise of the phantom at CT was measured to quantify the degree of metal artifacts generated by the spinal screws. Noise was defined as the standard deviation (SD) of the CT numbers expressed in HU. A radiologist placed a total of six circular ROIs (three for each set of spinal screws) in the area in which the image was most severely affected by the metal artifacts near the screws (Fig. 2). The mean area of the ROIs was 2.07 cm^2 (range 1.33–2.53 cm^2). ROIs were placed in identical areas in all four reconstructed images using the copy-and-paste function of the software. SD of the CT numbers at each ROI in each reconstructed image was measured as the marker of noise and were compared between the four reconstructed images. All ROI measurements were performed using PACS software (Maroview 5.4, Infinitt Healthcare, Seoul, South Korea).

Clinical study

Patients

From September 2017 to December 2017, a total of 47 patients (26 men, 21 women; age range 42–87 years; mean, 67.9 years) with metallic prostheses in the abdominopelvic region underwent abdominopelvic CT scans using a dual-layer, dual-energy CT scanner (IQon spectral CT, Philips Healthcare, Best, The Netherlands). Of the 47 patients, 36 had spinal prostheses and 11 had hip prostheses. Indications for CT were variable, but most patients (34/47 patients, 72.3%) underwent CT for work-up or surveillance for malignancies (hepatocellular carcinoma in 11 patients, stomach cancer in 9, colorectal cancer in 7, periampullary cancer in 2, breast cancer in 2, pancreatic cancer in 1, ovarian cancer in 1, and lymphoma in 1). Other indications for CT were surveillance for chronic hepatitis or liver cirrhosis in four patients, follow-up for pancreatitis in three, work-up for abdominal pain in two, a pancreatic mass in two, Crohn's disease in one, and a perianal mass in one.

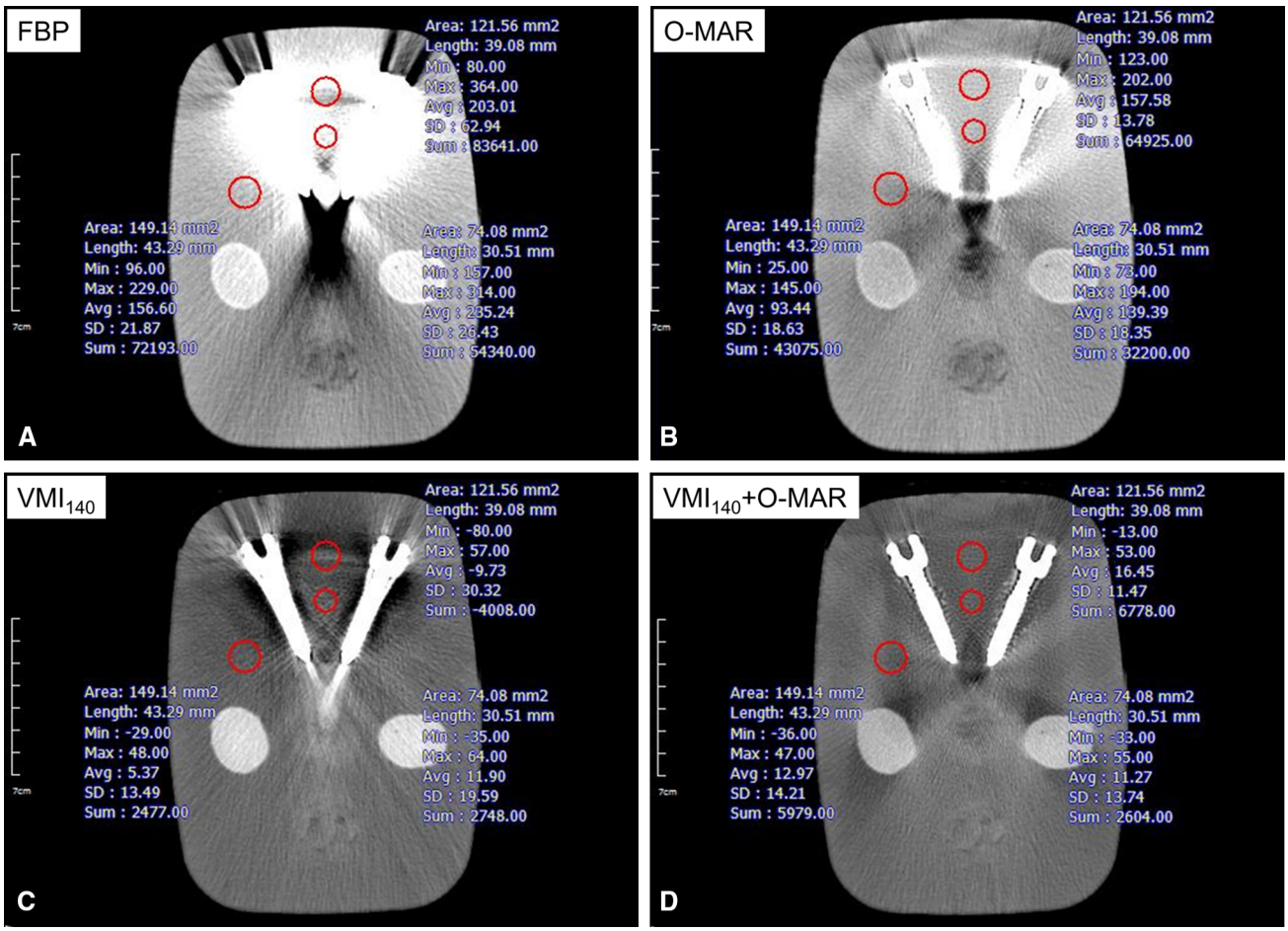

Fig. 2. Examples of image noise measurements in circular ROIs in the phantom CT reconstructed with **A** FBP, **B** O-MAR, **C** VMI_{140}, and **D** VMI_{140} + O-MAR. Standard deviation (SD) of the CT numbers expressed in HU was measured as image noise.

CT acquisition

CT protocols were variable: single portal venous phase in 10 patients or multiphases with two (n = 3), three (n = 13), or four (n = 21) phases. However, as all CT protocols included portal venous phase images, portal venous phase images were used to analyze the metal artifacts. 1.5 mL/kg of a 350 mg·I/mL iodinated contrast agent was administered for 30 s. A fixed delay of 60–70 s was used for the portal venous phase. Other scanning parameters were as follows: detector configurations, 64 × 0.625 mm; tube voltage, 120 kVp; tube current, 71–187 mAs using automatic exposure control; pitch, 0.797; rotation time: 0.33 s; matrix, 512 × 512; slice thickness, 2 or 3 mm; and reconstruction interval, 2 mm. To evaluate the effect of VMI and O-MAR in metal artifact reduction, all CT images in the portal venous phase were reconstructed in the same manner as that in the phantom study.

CT image analysis

All CT images were analyzed both qualitatively and quantitatively. For qualitative analysis of the CT images, two radiologists (E.K.H. with 3 years of experience and J.S.B. with 7 years of experience) independently evaluated the CT images. Information regarding the reconstruction method could not be blinded as CT images using different reconstruction methods are clearly able to be discerned by the radiologists. First, the degree of metal artifacts was graded by the radiologists on a 4-point scale: (1) severe artifacts obscuring abdominal organs or vessels and non-diagnostic; (2) moderate artifacts obscuring abdominal organs or vessels but diagnostic; (3) mild artifacts not obscuring abdominal organs or vessels; and (4) absent. The radiologists also chose the best image for reading among the four reconstructed images (FBP, O-MAR, VMI_{140}, and VMI_{140} + O-MAR). Second, the radiologists reported whether or not any potential diagnostic improvement of the images was depicted. If there was any potential diagnostic improvement, the type of the improvement was reported as follows: better depiction of abdominal organs; better skin delineation; decreased beam-hardening or photon starvation artifacts; or a combination of any of the above. Third, the radiologists reported whether there were O-MAR-related artifacts in the images reconstructed with O-MAR. O-MAR-related artifacts were categorized into the following subtypes: mild but thicker streak artifacts; abnormal delineation of bone-like structures; changes in the attenuation of normal tissue; or a combination of any of the above. Finally, the radiologists determined whether there was any diagnostic benefit using O-MAR and VMI. If there was any diagnostic benefit, the details of the diagnostic benefit were reported.

Quantitative analysis of the images was performed in a similar manner to that of the phantom study. A radiologist placed a total of three circular ROIs in the area in which the image was most severely affected by the metal artifacts. ROIs were located within the soft tissue (either fat or muscle) near the prostheses and particular attention was paid so as not to include areas of air or bone. The mean area of the ROIs was 1.90 cm^2 (range 1.21–3.08 cm^2). ROIs were placed in identical areas in all four reconstructed images using the copy-and-paste function of the software program. Noise of the images was measured as the mean SD of the three ROIs and were compared among the four reconstructed images (FBP, O-MAR, VMI_{140}, and VMI_{140} + O-MAR).

To evaluate the effect of reduced contrast created by iodine-based contrast agents in VMI_{140}, a radiologist (J.H.P) placed other five circular ROIs in the abdominal aorta, portal vein, hepatic parenchyma, paraspinal muscle, and subcutaneous fat on the images. ROIs were placed in identical areas in all four images using the copy-and-paste function of the software program. Areas affected by metal artifact were avoided as much as possible. Mean HU of each ROI was measured in all four images, and the difference of HU between hepatic parenchyma and back muscle, abdominal aorta, and portal vein was calculated to evaluate the contrast between less-enhancing, well-enhancing organs, and vessels. All ROI measurements were performed using the same PACS software used in the phantom study.

Statistical analysis

The Friedman test was used to compare the noise of the images among the four reconstruction methods in the phantom study and the Wilcoxon signed-rank test was used to perform a pairwise comparison. In the clinical study, one-way repeated-measures analysis-of-variance (ANOVA) was performed to compare the noise and grade of the metal artifacts of the images among the four reconstruction methods. The Scheffe test was used as a post hoc test to perform a pairwise comparison. Paired t test or the Wilcoxon signed-rank test was used to compare the contrast enhancement among the four CT images according to the normality. A two-sided $P < 0.05$ was considered to indicate a statistically significant difference. All statistical analyses were carried out using SPSS software version 23 (IBM Corp., Armonk, NY, USA).

Results

Phantom study

Noise defined as the SD of the CT numbers in the four different reconstruction methods is illustrated in Fig. 3a. Mean noise expressed as the averaged SD of the six ROIs were 62.4 ± 15.7, 26.4 ± 8.5, 25.0 ± 5.8, and 16.3 ± 3.7

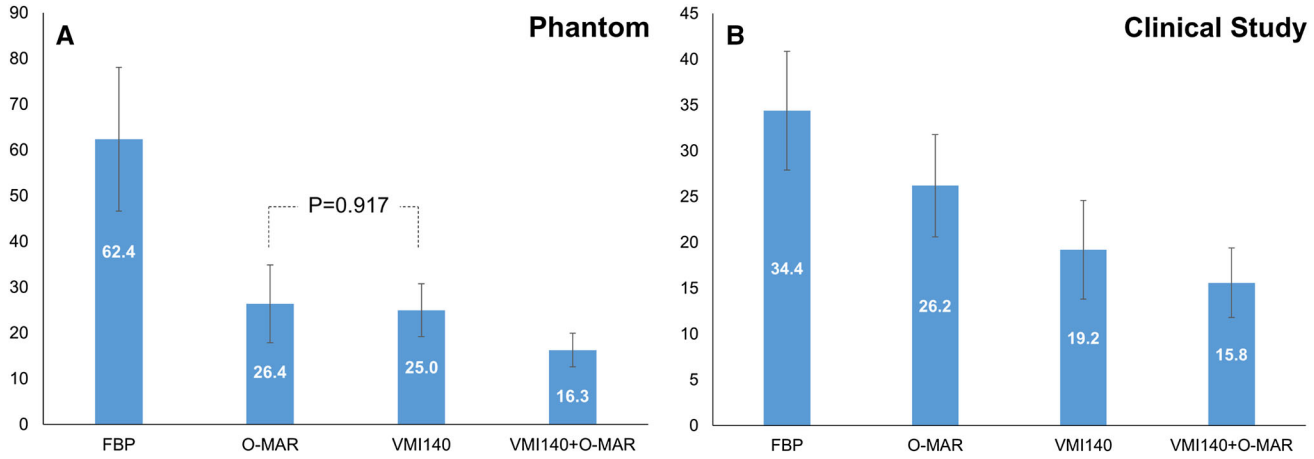

Fig. 3. Graph showing the image noise in the phantom CT (**A**) and clinical abdominal CT images (**B**) reconstructed using four different methods. **A** In the phantom study, differences in image noise were statistically significant ($P = 0.028$), except between O-MAR and VMI_{140} ($P = 0.917$). **B** In the clinical study, all pairs showed a significant difference in pairwise comparisons ($P \leq 0.025$).

HU in the CT images reconstructed with FBP, O-MAR, VMI_{140}, and VMI_{140} + O-MAR, respectively. The Friedman test showed that there were statistically significant differences in image noise among the four reconstruction methods ($P = 0.001$). In the pairwise comparison, noise was demonstrated to be significantly reduced when VMI_{140} or O-MAR was applied compared to FBP and further reduced when both were applied in conjunction (all Ps = 0.028). However, the noise was similar between O-MAR and VMI_{140} (P = 0.917).

Clinical study

The results of quantitative analysis are summarized in Fig. 3b. Mean noise were 34.4 ± 6.5, 26.2 ± 5.6, 19.2 ± 5.4, and 15.8 ± 3.8 HU in the CT images reconstructed with FBP, O-MAR, VMI_{140}, and VMI_{140} + O-MAR, respectively, and were significantly different among the four reconstruction methods ($P < 0.001$). All pairs also showed statistically significant differences at pairwise comparisons ($P \leq 0.025$) with VMI_{140} + O-MAR demonstrating the lowest noise.

Qualitative analysis also demonstrated that metal artifacts were significantly reduced when VMI and O-MAR were applied in conjunction ($P < 0.001$). The mean degree of artifacts graded by the radiologists were 1.04 ± 0.20, 2.13 ± 0.54, 2.36 ± 0.79, 2.85 ± 0.62 for reviewer 1 and 1.53 ± 0.58, 2.04 ± 0.41, 2.26 ± 0.61, 2.87 ± 0.40 for reviewer 2 in the CT images reconstructed with FBP, O-MAR, VMI_{140}, and VMI_{140} + O-MAR, respectively (Table 1). The degree of metal artifacts was significantly different among the four reconstruction methods ($P < 0.001$). Pairwise comparisons showed similar results to that of the phantom study in that metal artifacts were significantly reduced when VMI or O-MAR was applied and further reduced when both were applied in conjunction ($P < 0.001$). However, the degree of metal artifacts between VMI and O-MAR did not show a significant difference for both reviewers ($P = 0.285$ for reviewer 1 and 0.255 for reviewer 2).

In terms of a best image, VMI_{140} + O-MAR was selected as the best image in 31 (66.0%) of 47 patients for reviewer 1 and 35 (74.5%) of 47 patients for reviewer 2. Using VMI_{140} + O-MAR, image quality improvement was observed in all 47 patients (Table 2). For reviewer 1, 43 of the 47 patients (91.5%) showed improvement in more than one category: two categories in 16 patients and all three categories in 27 patients. For reviewer 2, 43

Table 1. Mean degree of artifacts graded by two radiologists in clinical abdominopelvic CT images reconstructed using four different methods ($n = 47$)

	Mean degree of artifacts	*P* value[a]		
		vs. FBP	vs. O-MAR	vs. VMI_{140}
Reviewer 1				
FBP	1.04 ± 0.20			
O-MAR	2.13 ± 0.54	< 0.001		
VMI_{140}	2.36 ± 0.79	< 0.001	0.285	
VMI_{140} + O-MAR	2.85 ± 0.62	< 0.001	< 0.001	0.001
P value[b]	< 0.001			
Reviewer 2				
FBP	1.53 ± 0.58			
O-MAR	2.04 ± 0.41	< 0.001		
VMI_{140}	2.26 ± 0.61	< 0.001	0.255	
VMI_{140} + O-MAR	2.87 ± 0.40	< 0.001	< 0.001	< 0.001
P value[b]	< 0.001			

FBP, filtered back-projection algorithm; O-MAR, metal artifact reduction for orthopedic implants; VMI_{140}, virtual monochromatic images obtained at 140 keV; VMI_{140} + O-MAR, virtual monochromatic images obtained at 140 keV with O-MAR

[a]The Scheffe test was used as a post hoc test to perform pairwise comparisons

[b]*P* values were obtained using the analysis of variance (ANOVA) test

Table 2. Image quality improvement in clinical abdominopelvic CT images using VMI_{140} + O-MAR assessed by two radiologists (n = 47)

Type of improvement	Number of patients (%)	
	Reviewer 1 (%)	Reviewer 2 (%)
1. Decreased beam-hardening or photon starvation artifacts	4 (8.5)	4 (8.5)
2. Better depiction of abdominal organs	0 (0)	0 (0)
3. Better skin delineation	0 (0)	0 (0)
Two categories (1 + 2 or 3)	16 (34.0)	39 (83.0)
All three categories (1 + 2 + 3)	27 (57.4)	4 (8.5)

VMI_{140} + O-MAR, virtual monochromatic images obtained at 140 keV with metal artifact reduction for orthopedic implants (O-MAR)

of the 47 patients (91.5%) also showed improvement in more than one category: two categories in 39 patients and all three categories in 4 patients. A representative example showing the aforementioned image quality improvement is shown in Fig. 4.

Using VMI_{140} + O-MAR in conjunction, actual diagnostic improvements were observed by both reviewers in three patients, who would otherwise have had a false-negative diagnosis. Post-operative fluid collection obscured by metal artifacts was clearly depicted only after VMI_{140} and O-MAR were applied together in one patient, metastatic retroperitoneal lymph nodes from periampullary cancer were more clearly depicted in another patient, and retroperitoneal lymphadenopathies due to lymphoma were more clearly depicted in the third patient. Representative examples are presented in Figs. 5 and 6.

Artifacts related to the O-MAR algorithm occurred in a total of 38 patients (38/47, 80.9%) by both reviewers. All of the 38 patients with O-MAR related artifacts had mild but thicker streak artifacts. In addition, one (for reviewer 1) or six (for reviewer 2) had abnormal delineation of bone-like structures and one (for reviewer 1) or eight (for reviewer 2) had changes in the attenuation of normal tissue. And three (for reviewer 2) had both abnormal delineation of bone-like structures and changes in the attenuation of normal tissue. However, none of these artifacts were observed to affect the diagnostic performance of the CT images.

Finally, mean HUs of ROIs at the five organs on FBP and VMI_{140} were summarized in Table 3. Data only for FBP and VMI_{140} were provided because the application of O-MAR did not affect the HU on the images at all. As expected, absolute HUs of enhancing organs (abdominal aorta, portal vein, hepatic parenchyma, and paraspinal muscle) were significantly decreased (all Ps < 0.001) when using VMI_{140}. In addition, the contrast between less-enhancing, well-enhancing organs, and vessels expressed by the differences of HU between liver and paraspinal muscle, abdominal aorta, and portal vein were significantly reduced (all Ps < 0.001).

Discussion

Image quality can be measured using various parameters such as spatial resolution, HU accuracy, alignment, or detectability. However, as image noise is also a key component of image quality [22], decreased image noise should be able to result in increased image quality. In this regard, our study results demonstrated that image noise was able to be significantly reduced by applying VMI with high keV (140 keV) or O-MAR compared to that using FBP alone. When both VMI and O-MAR were applied in conjunction, image noise was further able to be decreased as compared to when VMI or O-MAR was applied alone. Thus, when possible, the use of both VMI and O-MAR is recommended for maximum metal artifact reduction, particularly in patients whom metal artifacts significantly deteriorate image quality, leading to a diagnostic challenge.

Not only noise, but the image quality evaluated by radiologists was also demonstrated to have significantly improved by applying either VMI or O-MAR compared to FBP alone. In addition, similar to the quantitative results, image quality was further able to be improved when both VMI and O-MAR were applied in conjunction. In particular, abdominal organs were more clearly depicted when both VMI and O-MAR were applied together, in most cases (40/47, 85%), which may help reduce the number of false negatives using images obscured by artifacts without applying VMI or O-MAR. Indeed, in our study, three cases demonstrated actual diagnostic improvement by revealing enlarged lymph nodes and post-operative complications, which had been obscured by artifacts without the use of VMI and O-MAR in conjunction. Therefore, we suggest that diagnostic improvement can be achieved via a reduction in the number of false-negative findings, especially in the retroperitoneum or pelvic cavity, by applying VMI and O-MAR together in patients with spinal or hip prostheses. To the best of our knowledge, this is the first report to analyze the additional effect of metal artifact reduction and the resultant potential diagnostic improvement using O-MAR and VMI in conjunction.

There are a few limitations to using O-MAR and VMI that we should be aware of. In the iterative loop of the O-MAR algorithm, there is a segmentation step to create images only consisting of pixels categorized as metal so as to identify projections that are contributed from metal [23]. However, this method can introduce its own new artifacts related to the algorithm, especially when reliable segmentation becomes impossible due to severe metal artifacts [24]. These new artifacts related to O-MAR are especially more likely to occur when the metal is located near low-density tissue or air since the

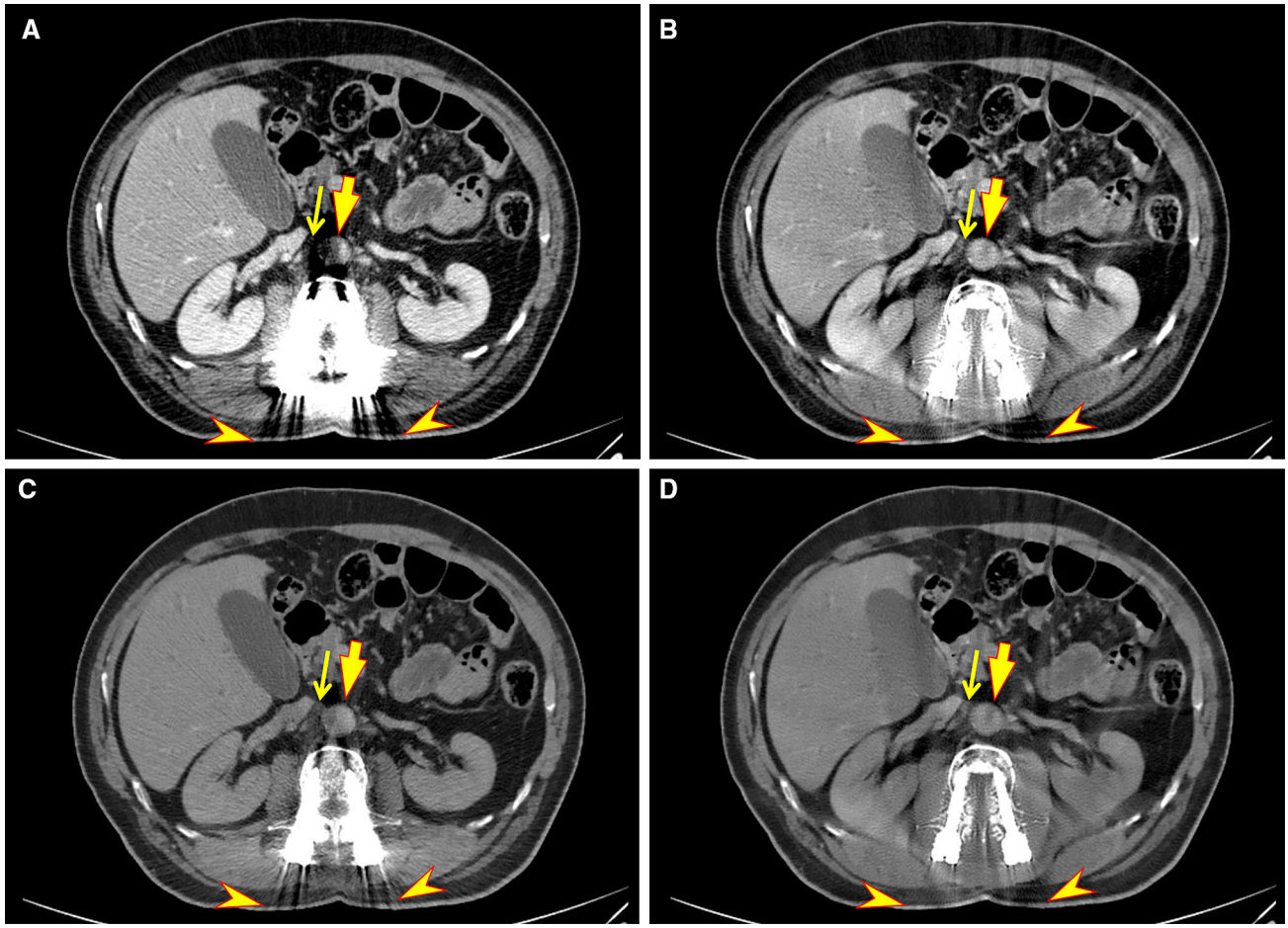

Fig. 4. A 71-year-old man who underwent spinal fixation at the lumbar spine. **A** CT image reconstructed with FBP shows severe metal artifacts which obscure parts of the aorta (arrow) and aortocaval space (thin arrow). Skin contour is also partly obscured by the metal artifacts (arrowheads). **B, C** CT images reconstructed with O-MAR (**B**) and VMI_{140} (**C**) show decreased metal artifacts with less obscured aorta (arrow), aortocaval space (thin arrow), and skin contour (arrowheads). Nonetheless, residual metal artifacts can be seen around the spine screws. **D** CT image reconstructed with VMI_{140} + O-MAR also clearly depicts the aorta (arrow), aortocaval lymph node (thin arrow), as well as the skin contour (arrowheads). Note that the metal artifacts around the spine screws were further reduced. Therefore, radiologists chose this image as the best image in terms of metal artifacts.

algorithm was optimized to correct for metal implants embedded into normal soft tissue [23]. Several clinical studies have already reported the creation of new artifacts related to iterative reconstruction methods, such as the pseudo-cemented appearance or streaks with O-MAR [16, 17] as well as other similar metal artifact reduction algorithms used by other vendors [25–27]. Indeed, such artifacts related to the O-MAR algorithm were observed in most of the patients (41/47, 87%) in our study, however, none of the O-MAR related artifacts were shown to significantly affect the diagnostic performance in our study. Nevertheless, the manufacturer recommended that clinicians should read the O-MAR images along with the conventional images without O-MAR [23]. As for VMI, a high keV (i.e., 140 keV) is known to reduce the contrast created by iodine-based contrast agents, which was consistent with our study results. Among the various keVs, the contrast-to-noise ratio (CNR) of iodine was the highest at 68 keV and gradually decreased along with increasing keV [28]. This decrease in the CNR of iodine may lower diagnostic performance by making it harder to detect and characterize enhancing lesions in the abdominopelvic cavity. However, this may also be overcome using conventional images obtained at 120 kVp which would be equivalent to 77 keV [29]. A cross-referenced review of two images may be more time-consuming in clinical practice, however, we believe that it may be acceptable considering the potential diagnostic improvement that can be obtained using O-MAR and VMI_{140} in conjunction, especially in problematic cases involving severe metal artifacts.

Finally, in our study, we used the CT machine which was designed specifically for spectral detector-based imaging. Therefore, upfront decision-making was not

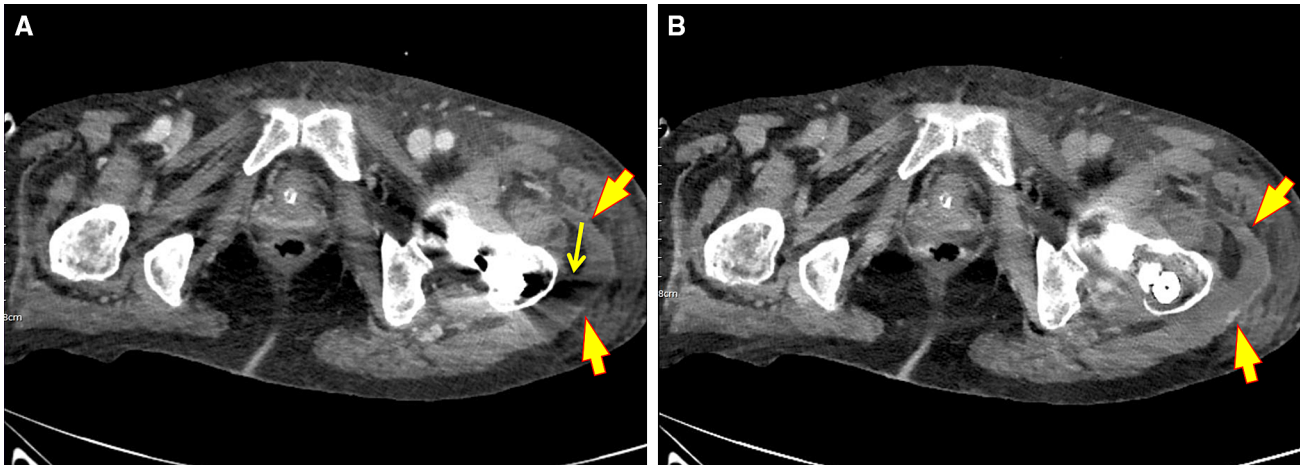

Fig. 5. Representative case showing actual diagnostic improvement using metal artifact reduction algorithms. An 87-year-old woman underwent intramedullary pinning in the femur 2 days ago. **A** On the CT image reconstructed with FBP, post-operative fluid collection (arrows) at the left lateral thigh is partially obscured by metal artifacts (thin arrow). **B** However, on the CT image reconstructed with VMI_{140} + O-MAR, this fluid collection (arrows) is clearly depicted after a reduction in metal artifacts.

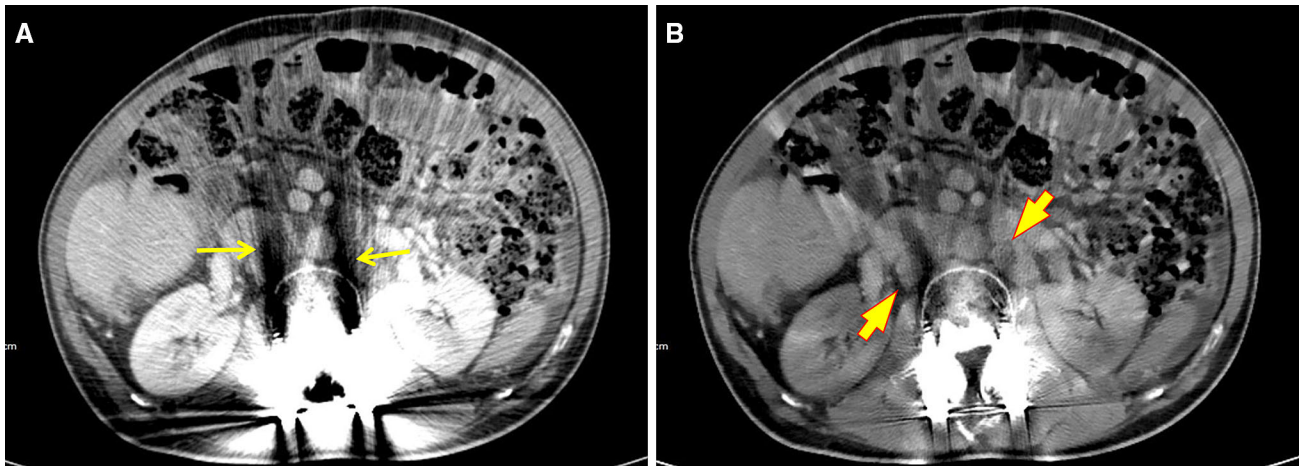

Fig. 6. Representative case showing actual diagnostic improvement using metal artifact reduction algorithms. A 53-year-old woman who underwent pylorus-preserving pancreaticoduodenectomy due to ampulla of Vater cancer had a spinal fixation. **A** On the CT image reconstructed with FBP, retroperitoneal lymph nodes are severely obscured by metal artifacts (thin arrows). **B** However, on the CT image reconstructed with VMI_{140} + O-MAR, these lymph nodes (arrows) are clearly demonstrated after a reduction in metal artifacts.

Table 3. Mean HU of the organs measured in FBP and VMI_{140} images (n = 47)

	FBP	VMI_{140}	P value[a]
1. Abdominal aorta	180.94 ± 21.72	73.92 ± 7.15	< 0.001
2. Portal vein	192.61 ± 22.96	76.45 ± 8.91	< 0.001
3. Hepatic parenchyma	120.78 ± 12.87	72.74 ± 7.17	< 0.001
4. Paraspinal muscle	66.36 ± 7.59	53.58 ± 6.33	< 0.001
5. Subcutaneous fat	− 93.76 ± 19.79	− 69.71 ± 14.15	< 0.001
1–3	60.16 ± 21.09	1.18 ± 8.73	< 0.001
2–3	71.83 ± 20.96	3.71 ± 9.80	< 0.001
3–4	54.42 ± 13.02	19.16 ± 8.12	< 0.001

HU, Hounsfield unit; FBP, filtered back-projection algorithm; VMI_{140}, virtual monochromatic images obtained at 140 keV
[a] P values were obtained using the paired t test

necessary to obtain spectral information owing to its ability to handle X-ray photons at the detector level. After obtaining spectral CT datasets, retrospective on-demand spectral analysis such as generation of VMI_{140} images allows radiologists to further reduce metal artifacts without additional radiation exposure. Indeed, the mean effective radiation dose (7.33 mSv, conversion coefficient estimated to 0.015) [30] of portal phase CT was lower than that of a single-energy CT study with a mean effective radiation dose of 10 (3.5–25) mSv [31].

There are several limitations in our study that should be mentioned. First, the number of patients included in our study was relatively small. However, this is the first

preliminary report describing the feasibility and potential for the combined use of monoenergetic high keV (VMI_{140}) images and the O-MAR. Therefore, we believe that a small number of patients are sufficient for this preliminary study and that further studies enrolling a large study populations are warranted to confirm our study results. Second, our reviewers performed qualitative analysis without being blinded to the information of whether O-MAR or VMI was applied, and this may have resulted in bias in evaluating which images provided the best image quality. However, blinding would be virtually impossible for this type of investigation as radiologists would easily be able to recognize whether O-MAR or VMI was applied while reviewing the images. Third, as most of the clinical indications were follow-up imaging or surveillance in cancer patients, many images were normal or just similar to the previously taken CT images. We believe that this may have been the reason why actual diagnostic improvement was observed in only three patients. We surmise that if more patients in wards or the emergency room had been included, more cases of actual diagnostic improvement may have been observed. Nevertheless, the fact that there were some cases where additional diagnoses were made possible by applying O-MAR and VMI in conjunction indicates the potential clinical usefulness of performing O-MAR and VMI together.

In conclusion, metal artifacts can be additionally reduced by applying O-MAR and VMI in conjunction, compared to their separate application, thereby improving diagnostic performance and reducing the number of false-negative results obscured by metal artifacts.

Compliance with ethical standards

Funding This study was supported by Philips Health Systems Korea.

Conflict of interest The authors declare that they have no conflict of interest.

Ethical approval All procedures performed in studies involving human participants were in accordance with the ethical standards of the institutional and/or national research committee and with the 1964 Helsinki declaration and its later amendments or comparable ethical standards. For this type of study formal consent is not required.

References

1. Bamberg F, Dierks A, Nikolaou K, et al. (2011) Metal artifact reduction by dual energy computed tomography using monoenergetic extrapolation. Eur Radiol 21(7):1424–1429
2. Barrett JF, Keat N (2004) Artifacts in CT: recognition and avoidance. Radiographics 24(6):1679–1691
3. Van Gompel G, Van Slambrouck K, Defrise M, et al. (2011) Iterative correction of beam hardening artifacts in CT. Med Phys 38(Suppl 1):S36
4. Mori I, Machida Y, Osanai M, Iinuma K (2013) Photon starvation artifacts of X-ray CT: their true cause and a solution. Radiol Phys Technol 6(1):130–141
5. Wang G, Vannier MW, Cheng PC (1999) Iterative X-ray cone-beam tomography for metal artifact reduction and local region reconstruction. Microsc Microanal 5(1):58–65
6. Wang G, Snyder DL, O'Sullivan JA, Vannier MW (1996) Iterative deblurring for CT metal artifact reduction. IEEE Trans Med Imaging 15(5):657–664
7. Kidoh M, Nakaura T, Nakamura S, et al. (2014) Reduction of dental metallic artefacts in CT: value of a newly developed algorithm for metal artefact reduction (O-MAR). Clin Radiol 69(1):e11–e16
8. Morsbach F, Wurnig M, Kunz DM, et al. (2013) Metal artefact reduction from dental hardware in carotid CT angiography using iterative reconstructions. Eur Radiol 23(10):2687–2694
9. Hsieh J, Molthen RC, Dawson CA, Johnson RH (2000) An iterative approach to the beam hardening correction in cone beam CT. Med Phys 27(1):23–29
10. Meinel FG, Bischoff B, Zhang Q, et al. (2012) Metal artifact reduction by dual-energy computed tomography using energetic extrapolation: a systematically optimized protocol. Invest Radiol 47(7):406–414
11. Yu L, Leng S, McCollough CH (2012) Dual-energy CT-based monochromatic imaging. AJR Am J Roentgenol 199(5 Suppl):S9–S15
12. Zhou C, Zhao YE, Luo S, et al. (2011) Monoenergetic imaging of dual-energy CT reduces artifacts from implanted metal orthopedic devices in patients with factures. Acad Radiol 18(10):1252–1257
13. Pessis E, Campagna R, Sverzut JM, et al. (2013) Virtual monochromatic spectral imaging with fast kilovoltage switching: reduction of metal artifacts at CT. Radiographics 33(2):573–583
14. An C, Chun YM, Kim S, et al. (2014) Dual-energy computed tomography arthrography of the shoulder joint using virtual monochromatic spectral imaging: optimal dose of contrast agent and monochromatic energy level. Korean J Radiol 15(6):746–756
15. Hu Y, Pan S, Zhao X, et al. (2017) Value and clinical application of orthopedic metal artifact reduction algorithm in CT scans after orthopedic metal implantation. Korean J Radiol 18(3):526–535
16. Shim E, Kang Y, Ahn JM, et al. (2017) Metal artifact reduction for orthopedic implants (O-MAR): usefulness in CT evaluation of reverse total shoulder arthroplasty. AJR Am J Roentgenol 209(4):860–866
17. Jeong S, Kim SH, Hwang EJ, et al. (2015) Usefulness of a metal artifact reduction algorithm for orthopedic implants in abdominal CT: phantom and clinical study results. AJR Am J Roentgenol 204(2):307–317
18. Huang JY, Kerns JR, Nute JL, et al. (2015) An evaluation of three commercially available metal artifact reduction methods for CT imaging. Phys Med Biol 60(3):1047–1067
19. Winklhofer S, Benninger E, Spross C, et al. (2014) CT metal artefact reduction for internal fixation of the proximal humerus: value of mono-energetic extrapolation from dual-energy and iterative reconstructions. Clin Radiol 69(5):e199–e206
20. Higashigaito K, Angst F, Runge VM, Alkadhi H, Donati OF (2015) Metal artifact reduction in pelvic computed tomography with hip prostheses: comparison of virtual monoenergetic extrapolations from dual-energy computed tomography and an iterative metal artifact reduction algorithm in a phantom study. Invest Radiol 50(12):828–834
21. Wang Y, Qian B, Li B, et al. (2013) Metal artifacts reduction using monochromatic images from spectral CT: evaluation of pedicle screws in patients with scoliosis. Eur J Radiol 82(8):e360–e366
22. Wilson JM, Christianson OI, Richard S, Samei E (2013) A methodology for image quality evaluation of advanced CT systems. Med Phys 40(3):031908
23. Philips Healthcare (2012) Metal artifact reduction for orthopedic implants (O-MAR). http://clinical.netforum.healthcare.philips.com/us_en/Explore/White-Papers/CT/Metal-Artifact-Reduction-for-Orthopedic-Implants-(O-MAR). Accessed 21 Feb 2018
24. Koehler T, Brendel B, Brown KM (2012) A new method for metal artifact reduction in CT. In: The International Conference in X-ray computed tomography. http://repository.tudelft.nl/assets/uuid:22d5815d-dcfe-48df-93a4-9d1c4e8e85fc/MS-33.229.pdf. Accessed 21 Feb 2018
25. Andersson KM, Nowik P, Persliden J, Thunberg P, Norrman E (2015) Metal artefact reduction in CT imaging of hip prostheses—an evaluation of commercial techniques provided by four vendors. Br J Radiol 88(1052):20140473

26. Andersson KM, Norrman E, Geijer H, et al. (2016) Visual grading evaluation of commercially available metal artefact reduction techniques in hip prosthesis computed tomography. Br J Radiol 89(1063):20150993
27. Han SC, Chung YE, Lee YH, et al. (2014) Metal artifact reduction software used with abdominopelvic dual-energy CT of patients with metal hip prostheses: assessment of image quality and clinical feasibility. AJR Am J Roentgenol 203(4):788–795
28. Matsumoto K, Jinzaki M, Tanami Y, et al. (2011) Virtual monochromatic spectral imaging with fast kilovoltage switching: improved image quality as compared with that obtained with conventional 120 kVp CT. Radiology 259(1):257–262
29. Brook OR, Gourtsoyianni S, Brook A, et al. (2013) Split-bolus spectral multidetector CT of the pancreas: assessment of radiation dose and tumor conspicuity. Radiology 269(1):139–148
30. Christner JA, Kofler JM, McCollough CH (2010) Estimating effective dose for CT using dose-length product compared with using organ doses: consequences of adopting International Commission on Radiological Protection publication 103 or dual-energy scanning. AJR Am J Roentgenol 194(4):881–889
31. Albert JM (2013) Radiation risk from CT: implications for cancer screening. AJR Am J Roentgenol 201(1):W81–W87